

Synthesis of ZnWO₄/Cu₂O Composites and Efficient Catalytic Properties for 4-nitrophenol Removal

Ziwei Wang

China West Normal University

Fengping Fu

China West Normal University

Qian He

China West Normal University

Ting Zhu

China West Normal University

Fang Liao (✉ [liaofang407@163.com](mailto:liao407@163.com))



China West Normal University <https://orcid.org/0000-0002-3024-9339>

Research Article

Keywords: 4-nitrophenol, Cu₂O matrix composites, ZnWO₄, Catalytic reduction

Posted Date: October 22nd, 2021

DOI: <https://doi.org/10.21203/rs.3.rs-1000941/v1>

License:   This work is licensed under a Creative Commons Attribution 4.0 International License. [Read Full License](#)

Abstract

Preparation of $\text{ZnWO}_4/\text{Cu}_2\text{O}$ composite materials by environmental protection experimental method. ZnWO_4 nanorods were prepared by a simple hydrothermal method, and then $\text{ZnWO}_4/\text{Cu}_2\text{O}$ composites were prepared by chemical precipitation method. The experimental method is simple and clean. Due to the unique structural characteristics of Cu_2O , the wide band gap of ZnWO_4 was improved and the $\text{ZnWO}_4/\text{Cu}_2\text{O}$ composite with better catalytic performance was generated. Various tests show that the catalytic performance and stability of $\text{ZnWO}_4/\text{Cu}_2\text{O}$ is not lower than that of ZnWO_4 . Among them, $\text{ZnWO}_4/\text{Cu}_2\text{O}$ -5 has the best catalytic degradation effect. The Cu-H generated during the degradation of 4-nitrophenol (4-NP) prevents the oxidation of Cu^+ , and the neutral product 4-aminophenol (4-AP) is easier to fall off, which improves its recycling efficiency. These encouraging results show that the $\text{ZnWO}_4/\text{Cu}_2\text{O}$ composites have great potential to degrade 4-NP.

1 Introduction

- 4-nitrophenol (4-NP) has high toxicity and long half-life in the natural environment, which causes serious pollution to the water environment. It is easy to accumulate in humans and animals to cause cancer or physical deformity [1, 2]. 4-aminophenol (4-AP) as the intermediate of 4-NP catalytic degradation is widely used in medicine, dyes, pesticides and other fields. Among many methods for reducing 4-NP to 4-AP, catalytic hydrogenation reduction method is the best, which has the advantages of high conversion efficiency and mild operating conditions [3]. Among them, noble metal nanoparticles have the best catalytic effect [4, 5]. But it is expensive, limited reserves and difficult to large-scale promotion. Scientists are more focused on the development of cheap, abundant non-precious metal catalysts.
- Cu_2O is a typical P-type direct band gap semiconductor material that can be excited by visible light. Its band gap is about 2.17 eV, and has good photoelectric properties [6, 7]. Cu_2O nanoparticles, not only has high photocatalytic activity, bactericidal activity, photoelectron conversion activity, but also has the advantages of high surface energy and large specific surface area [8]. This makes Cu_2O have applications in photocatalysis [9], photohydrolysis of hydrogen in aquatic products [10], CO oxidation [11], CO_2 reduction [12], and gas sensing [13]. However, the band gap of Cu_2O is narrow. And its reaction rate is slow, easy to be oxidized, low cycle utilization. In order to eliminate these shortcomings, researchers have made many efforts.
- Since scientists found ZnWO_4 , people have had a strong interest in it. ZnWO_4 is a wide band gap semiconductor photocatalyst. Zn^{2+} and W^{6+} have electronic configurations of d^{10} and d^0 , and are located at the centers of ZnO_6 and WO_6 . Therefore, they have high electron mobility, which have a matching valence band relationship with Cu_2O [14]. In this experiment, $\text{ZnWO}_4/\text{Cu}_2\text{O}$ composites are prepared according to the band gap characteristics of the two. Explore whether the photocatalytic properties of composite materials have improved.
- Therefore, in this study, ZnWO_4 nanorods with stable structure were prepared by simple hydrothermal method, and $\text{ZnWO}_4/\text{Cu}_2\text{O}$ was prepared by chemical precipitation method. Encouraging experimental

results have been obtained, among which $\text{ZnWO}_4/\text{Cu}_2\text{O}$ -5 has the best catalytic degradation effect. The modified catalyst improved the separation ability of electron-hole and enhanced the photocatalytic activity. The oxidation of Cu^+ was prevented by Cu-H generated in the catalytic degradation process. The neutral degradation product 4-AP made it easier to fall off and improved its recycling efficiency. The efficient recycling of $\text{ZnWO}_4/\text{Cu}_2\text{O}$ -X is in line with the concept of environmental protection, which is a more economical and feasible process. and the $\text{ZnWO}_4/\text{Cu}_2\text{O}$ catalyst is characterized by XRD, SEM, UV-Vis, TEM, XPS and HRTEM to determine the nature of catalytic activity of catalyst.

2 Experimental

2.1 Materials

Zinc nitrate hexahydrate and copper acetate monohydrate were purchased from Chengdu Kelong reagent plant. Sodium tungstate dihydrate was purchased from Tianjin Ruijinte Chemical Co., Ltd.. Sodium hydroxide and barium sulfate were purchased from Shandong Xiya Chemical Industry Co., Ltd.. Anhydrous glucose was purchased from Aladdin Reagent (Shanghai) Co., Ltd., and anhydrous ethanol was purchased from Tianjin Fuchen Chemical Reagent Plant. All chemical reagents were analytically pure.

2.2 $\text{ZnWO}_4/\text{Cu}_2\text{O}$ composites preparation

2.2.1 ZnWO_4 nanorods preparation

ZnWO_4 nanorods were prepared by hydrothermal method. 15 ml 6.7 M $\text{Na}_2\text{WO}_4 \cdot 2\text{H}_2\text{O}$ solution was dropped into 15 ml 6.7 M $\text{Zn}(\text{NO}_3)_2 \cdot 6\text{H}_2\text{O}$ solution. The pH was adjusted to 9 with an intelligent pH meter, stirred for 30 min, and transferred to a stainless steel autoclave. The temperature was adjusted to 453 K for 12 h. After the reaction, the precipitate was collected and washed several times with deionized water and anhydrous ethanol. Then the sample was dried by vacuum drying box, and the powder was grinded by bowl after drying.

2.2.2 $\text{ZnWO}_4/\text{Cu}_2\text{O}$ -X composites preparation

ZnWO_4 (0.0039 g, 0.0117 g, 0.0195 g, 0.0273 g) were added into $(\text{CH}_3\text{COO})_2\text{Cu} \cdot \text{H}_2\text{O}$ aqueous solution of 25 ml 0.05 M (X = 1, 3, 5, 7) for 30 min. Then stir at 313 K for 10 min, slowly drop 4 ml 1 M NaOH, stir at constant temperature for 10 min, add 15 ml 1 M glucose, stir at constant temperature for 2 h. The samples were obtained, and washed with deionized water and anhydrous ethanol several times, dried in vacuum dryer. The process is demonstrated in Fig. 1 .

Fig. 1 Preparation process of $\text{ZnWO}_4/\text{Cu}_2\text{O}$ composite

2.3 $\text{ZnWO}_4/\text{Cu}_2\text{O}$ -X composites characterization

Tecnai G2F30 transmission electron microscope (TEM) and high-resolution transmission electron microscope (HRTEM) were used for transmission. UV-Vis diffuse reflectance spectra were measured by UV-

3600 spectrophotometer. The scanning range was from 200 nm to 800 nm. The crystal phase of the sample was characterized by BRUCKER D8ADVANCE X-ray powder diffractometer in the range of 10–80°. X-ray diffraction (XRD) was performed with a 250Xi diffractometer. The energy spectrum was analyzed by SU8020 field emission scanning electron microscope (SEM).

2.4 Evaluation of catalysts performance

2.4.1 Catalytic activity for hydrogenation of catalyst test

10 mg catalyst was dissolved in 10 ml deionized water, and ultrasonic dispersion was uniform. 10 ml 0.24 M NaBH₄ aqueous solution was added to 90 ml 2.2×10⁻⁴ mol/L 4-NP. 0.02 ml catalyst solution was accurately removed by liquid gun and added to the above mixed solution. Add the catalyst and start timing. Remove 3.5 ml of solution every other time in the colorimetric dish. The ultraviolet spectrophotometer was immediately used to monitor the change of 4-NP ion absorption peak at 400 nm of purple wavelength in the scanning range of 250 nm–500 nm. The reaction rate constant is calculated by absorbance. The whole process was continuously stirred in a constant temperature water bath at 25°C.

2.4.2 Hydrogenation catalyst stability test

5 ml of 4-NP and 5 ml of NaBH₄ were mixed and diluted to 100 ml, and 0.2 ml of 1 mg/ml catalyst was added. The intensity of the absorption peak of the solution was detected by UV spectrophotometer at a certain interval. The stability of the solution was tested by repeated dripping. 1 ml of 1×10⁻² mol/L 4-NP was added at each reaction and repeated 15 times.

3 Results And Discussion

3.1 Morphology and microstructure analysis

Fig. 2 SEM images of **(a-b)** ZnWO₄; **(c-d)** Cu₂O; **(e-f)** ZnWO₄/Cu₂O

ZnWO₄ SEM images prepared by hydrothermal method are shown in **Fig. 2a** and **b**. The results show that the size of ZnWO₄ nanorods is uniform and the diameter is about 50 nm. **Fig. 2c** and **d** show that the Cu₂O spheres synthesized by chemical precipitation method are about 500 nm to 900 nm, and the surface is rough and not smooth, which greatly improves its activity. ZnWO₄/Cu₂O composites formed by chemical precipitation method are shown in **Fig. 2e** and **f**. It can be seen that ZnWO₄ is closely adhered to the surface of Cu₂O and does not change its morphology. Close contact ensures the effective transfer of charge during catalytic hydrogenation reduction. The mapping of ZnWO₄/Cu₂O is shown in Fig. 3, which shows that Zn, O, Cu and W exist in ZnWO₄/Cu₂O, and are uniformly distributed in the sample.

The TEM and HRTEM images of ZnWO₄/Cu₂O composites are shown in **Fig. 4**. According to **Fig. 4**, the lattice spacing of Cu₂O is 0.24 nm, which corresponds to 111 planes. The lattice spacing of 0.37 nm corresponds to 011 plane of ZnWO₄. At the same time, as shown in **Fig. 4c**, clear stripe spacing proves that Cu₂O and ZnWO₄ have good crystallinity, and they have matching crystal plane spacing and lattice plane.

3.2 Material composition and valence analysis (XRD and XPS)

As shown in **Fig. 5**, the black curve is ZnWO₄ nanowires. Its characteristic diffraction peaks are about 23.8°, 24.6°, 30.7°, 36.3°, 41.2°, 53.6°. Which are matched with (110), (200), (210), (211), (220), (310), (222), (320), (321), (400) and (421) crystal planes of ZnWO₄ (JCPDS NO.15-0774) [15]. The red curve is Cu₂O. Its characteristic diffraction peaks are 29.6°, 36.5°, 42.4°, 61.6°, 73.7°, corresponding to the (110), (111), (200), (220), (311) crystal planes of Cu₂O crystal. Which are consistent with the (JCPDS NO.77-0119) [29] card. When ZnWO₄/Cu₂O-X composite is synthesized, with the increase of ZnWO₄, the XRD pattern of ZnWO₄/Cu₂O-X composite does not appear the characteristic peak of ZnWO₄. There is only the narrow and sharp peak of Cu₂O, but the peak position is shifted. No other changes were detected, indicating the high purity of the complex. The main reason for the absence of ZnWO₄ characteristic peaks may be the content and particle size. The content of Zn and Cu in the synthesized compound were determined by inductively coupled plasma atomic emission spectrometer (ICP-OES), and the results are shown in **Table. 1**. The low content and high dispersion of ZnWO₄ can not cause the morphological change of Cu₂O, which is consistent with the results of SEM and TEM.

Table 1
The ratio of the amount of Zn/Cu in the ZnWO₄/Cu₂O compositee

catalyst	theoretical value	actual value
ZnWO ₄ /Cu ₂ O-1	1%	1.3%
ZnWO ₄ /Cu ₂ O-3	3%	4.0%
ZnWO ₄ /Cu ₂ O-5	5%	6.8%
ZnWO ₄ /Cu ₂ O-7	7%	9.4%

Fig. 5 XRD patterns of ZnWO₄; Cu₂O; ZnWO₄/Cu₂O-X

The characteristic peaks of Zn, W, O, Cu can be observed are shown in **Fig. 6**. **Fig. 6b** shows the spectra of Zn 2p, showing two peaks of 1021.9 eV and 1044.7 eV, corresponding to Zn 2p_{3/2} and Zn 2p_{1/2}, respectively. **Fig. 6c** is the XPS spectrum of W4f, showing two peaks of 35.8 eV and 37.9 eV, corresponding to W 4f_{7/2} and 4f_{5/2}, which determines the existence of W 4f. **Fig. 6d** is O, showing three peaks at 530.3 eV, 531.1 eV and 532.2 eV. The peak at 530.3 eV corresponds to the lattice oxygen in Cu₂O, and the peak at 531.1 eV corresponds to the lattice oxygen in ZnWO₄. The spectral result of Cu 2p is shown in **Fig. 6e**. There are two peaks at 932.9 eV and 952.3 eV, corresponding to Cu 2p_{3/2} and Cu 2p_{1/2}. XRD and XPS analysis showed that Cu₂O and ZnWO₄ coexist in Cu₂O/ZnWO₄.

Fig. 6 a XPS survey spectra; High-resolution XPS spectra of b Zn 2p; c W 4f; d O 1s and e Cu 2p

3.3 N₂ adsorption-desorption characterization of catalysts

The N₂ adsorption-desorption isotherms of Cu₂O and ZnWO₄/Cu₂O and their corresponding pore size distribution curves are shown in Fig. 7. It can be seen that Cu₂O and ZnWO₄/Cu₂O are typical type IV isotherms, indicating that Cu₂O and ZnWO₄/Cu₂O are mesoporous materials. In 0~0.9 V, the adsorption capacity of ZnWO₄/Cu₂O is low. While in the 0.9~1.0 V, the adsorption capacity is greatly improved. On the whole, the adsorption capacity of ZnWO₄/Cu₂O is low, indicating that the specific surface area is not large. But ZnWO₄/Cu₂O has stronger adsorption capacity than Cu₂O, indicating that its specific surface area is larger than Cu₂O. Which is consistent with the test results. The BET algorithm shows that the specific surface area of Cu₂O is 1.9 m²/g, and that of ZnWO₄/Cu₂O is 2.7 m²/g. The average pore sizes are 4.2 nm and 6.4 nm, and the pore volumes are 1.3×10⁻³ cm³/g and 2.8×10⁻³ cm³/g, respectively. It indicates that the combination of the two is conducive to improving the specific surface area, pore size and pore volume, but the space for improvement is very small.

Fig. 7 N₂ adsorption and desorption curves of a Cu₂O; b ZnWO₄/Cu₂O

3.4 Activity detection of catalysts

The activity of the catalyst was determined by the degradation degree of 4-NP by the catalyst. The standard schematic diagram of catalytic reduction of 4-NP are shown in Fig. 8a. Under neutral and acidic conditions, the peaks of 4-NP at about 317 nm. When NaBH₄ is added, the solution is alkaline. 4-NP is dissociated into ions, and the maximum absorption peak shifts to 400 nm. When the catalyst is added, 4-AP is rapidly generated. And its characteristic absorption peak is at 300 nm. There is no by-product in the whole reaction process [16]. The absorbance spectra of ZnWO₄, Cu₂O, ZnWO₄/Cu₂O-1, ZnWO₄/Cu₂O-3, ZnWO₄/Cu₂O-5, ZnWO₄/Cu₂O-7 changes with time are shown in Fig. 8(b-g). It can be seen from Fig. 8b that when ZnWO₄ is added, the absorbance almost don't change, which proved that ZnWO₄ is no catalytic. When other catalysts are added, the absorbance changes obviously. The degradation efficiency of ZnWO₄/Cu₂O composite for 4-NP is better than that of Cu₂O. The catalytic degradation efficiency from high to low are ZnWO₄/Cu₂O-5, ZnWO₄/Cu₂O-3, ZnWO₄/Cu₂O-7, ZnWO₄/Cu₂O-1, Cu₂O. Therefore, the combination of the two can modify Cu₂O and improve the catalytic activity of Cu₂O.

In order to more intuitively observe the influence of ZnWO₄/Cu₂O-X on the catalytic performance, we selected the absorbance at 400 nm to calculate the value of C_t/C₀ for comparison (C₀ and C_t are the concentration of 4-NP solution at time 0 and time t). As the reaction proceeds, the ratio of C_t/C₀ to time t becomes smaller and smaller. Which indicates that the content of 4-NP in the whole reaction system becomes lower and lower. The linear fitting of Fig. 8a show the linear relationship was good and conforms to the first-order kinetics. So (A₀ and A_t are the absorbance of 4-NP solution at 0 and t, K_{app} is the apparent rate constant, t is the reaction time):

$$\ln (A_t/A_0) = \ln (C_t/C_0) = -k_{app}t$$

The relationship between C_t/C_0 and t is shown in **Fig. 9a**. It can be seen that the conversion rate of $ZnWO_4/Cu_2O-5$ is the highest and that of Cu_2O is the lowest at the same time. So the catalytic activity of $ZnWO_4/Cu_2O-5$ is higher than that of Cu_2O .

The relationship between $\ln(C_t/C_0)$ and t is shown in **Fig. 9b**. It can be seen that the reaction rate of $ZnWO_4/Cu_2O-5$ is the fastest. Linear slopes were obtained by linear fitting. The k_{app} values of Cu_2O , $ZnWO_4/Cu_2O-1$, $ZnWO_4/Cu_2O-3$, $ZnWO_4/Cu_2O-5$ and $ZnWO_4/Cu_2O-7$ were $8.2 \times 10^{-3} s^{-1}$, $15.91 \times 10^{-3} s^{-1}$, $25.2 \times 10^{-3} s^{-1}$, $20.6 \times 10^{-3} s^{-1}$ and $6.2 \times 10^{-3} s^{-1}$, respectively. In order to show the advantages of composites more clearly, the activation factors of $ZnWO_4/Cu_2O-5$ were calculated by formula 2.

$$k' = k_{app} / m^2$$

Fig. 9 Different catalysts of **a** C_t/C_0 curve graph with time; **b** netic fitting graph

The results showed that the activation factors of Cu_2O and $ZnWO_4/Cu_2O-5$ were $31 \times 10^{-3} s^{-1} mg^{-1}$ and $126 \times 10^{-3} s^{-1} mg^{-1}$, respectively, indicating that its catalytic performance was better than that of most catalysts. As shown in **Table. 2**.

Table 2
Comparison of the rate constant (k) and activity factor (k') of different catalysts used to reduce 4-NP to 4-AP

sample	catalyst dosage	The concentration of NaBH ₄ (M)	[4-NP] usage (mM)	reaction rate constant (k)×10 ⁻³ (s ⁻¹)	active factors (k')×10 ⁻³ s ⁻¹ mg ⁻¹	references
5.1wt% Co-doped CuO NPs	1	8	0.12	43.80	43.8	[20]
Cu ₂ O NPs	1	0	0.1	15.7	15.7	[21]
Cu ₂ O/MoS ₂ /rGO	10	6.25	12.5	62	6.2	[22]
Cu ₂ O/Cu-MOF/rGO	1	100	0.1	32.7	32.7	[23]
Cu ₂ O/ZrO ₂	12	30	0.0625	15.97	1.331	[24]
15-cco/bv	1	50	0.1	24.8	24.8	[25]
Fe ₃ O ₄ @ppy-MAA/Ag	7.5	100	40	2.383	0.3177	[26]
Pt-NiO/G	1	100	0.1	33.9	33.9	[27]
Ag-Fe bimetallic NPs	5	3.333	0.0667	1.1	0.22	[28]
Cu ₂ O/ZnWO ₄ -5	0.2	0.025	0.2	25.2	126	This work

Fig. 10a The cycle stability test of ZnWO₄/Cu₂O-5 and **b** the time required for ZnWO₄/Cu₂O-5 to convert the same quality 4-NP

Finally, the stability test was carried out. Due to the small amount of catalyst, in order to avoid the loss caused by recycling, the stability of the catalyst was verified by adding 4-NP repeatedly. The specific operation steps were shown in Section 2.4.2. The relationship between C_t/C₀ and t in the 15 cycles is shown in **Fig. 10a**. It can be

seen from the figure that after 15 cycles, the degradation effect changed little, still reaching more than 95%. It indicates that catalytic stability was good. The time needed to convert the same mass of 4-NP is shown in **Fig. 10b**. It can be seen from the figure that the time used increases with the increase of cycles. But it remains unchanged after increasing to a certain extent, which indirectly indicates that it has good cycle stability.

3.5 Effect of reaction temperature on catalytic hydrogenation of 4-NP

In order to study the effect of temperature on the activity of the catalyst, the activity tests are carried out at 10°C, 25°C, 40°C, 55°C and 70°C (**Fig. 11a**), and their k values were obtained by linear fitting of kinetics (**Fig. 11b**). Which are $10.88 \times 10^{-3} \text{ s}^{-1}$, $25.20 \times 10^{-3} \text{ s}^{-1}$, $24.42 \times 10^{-3} \text{ s}^{-1}$, $31.93 \times 10^{-3} \text{ s}^{-1}$ and $31.49 \times 10^{-3} \text{ s}^{-1}$, respectively. It can be seen that the variation is large at low temperature, but not obvious at high temperature. It indicates that temperature has some influence on activity of the catalyst. The catalytic effect remained unchanged after the temperature

reached a certain level in the high temperature stage, and 50°C was the critical point.

Fig. 11a The relationship between C_t/C_0 and time at different temperatures and

b kinetic fitting graph

3.6. Valence analysis of catalyst elements before and after reaction

In order to study the reaction mechanism of 4-NP conversion to 4-AP, the $\text{ZnWO}_4/\text{Cu}_2\text{O}$ after reaction is characterized by XPS. The full spectrum of $\text{ZnWO}_4/\text{Cu}_2\text{O}$ shown in **Fig. 12a** indicates that there is no additional impurity element after the reaction. **Fig. 12b** and **c** shows that peaks of Zn 2p are 1021.7 eV (Zn $2p_{3/2}$) and 1044.8 eV (Zn $2p_{1/2}$), and the peaks of W 4f are 35.3 eV (W $4f_{7/2}$) and 37.5 eV (W $4f_{5/2}$). Compared with **Fig. 6a** and **b**, the spectral peaks of W4f move slightly. But there is one more peak in O 1s and Cu 2p, and the peak is 532.4 eV, indicating the formation of CuO. The peaks at 934.7 eV, 954.6 eV and 943.3 eV, 962.5 eV also indicate the formation of CuO in **Fig. 12e**. The peaks at 932.4 eV and 952.2 eV are Cu^+/Cu . Since it is difficult to distinguish the two by XPS, the valence state of copper ions can only be determined by X-ray induced Auger electron spectroscopy (XAES). The obtained figure shows three independent peaks. The main peak at about 570 eV is considered to represent Cu^+ , while the peak at about 567 eV is considered to represent CuO [17, 18]. The ratio of peak area of Cu_2O to Cu in the catalyst decreased from 3.57 to 2.43 before and after the reaction, and the presence of CuO indicated the formation of Cu. Sasmal et al. [19] reported that Cu_2O was easily reduced to Cu by NaBH_4 at pH about 9, while Cu was easily oxidized to CuO, and finally formed ternary complexes. The presence of Cu is very important for the reduction of 4-NP, which can absorb hydrogen and is the action site of BH_4^- . The shift of the binding energy peaks of Zn 2p and W 4f and the generation and shift of the binding energy peaks of O 1s and Cu 2p indicate that they interact.

Fig. 12a The XPS survey spectrum of the recycled $\text{ZnWO}_4/\text{Cu}_2\text{O}$; the high-resolution XPS spectra for **b** Zn 2p, **c** W 4f, **d** O 1s, **e** Cu 2p, **f** Cu LMM of the refreshed and **g** the used Cu LMM

3.7 Electrochemical impedance performance test

In order to study the charge transfer process and the separation efficiency of charge carriers, electrochemical impedance spectroscopy (EIS) was performed on Cu_2O , ZnWO_4 and $\text{ZnWO}_4/\text{Cu}_2\text{O}$. In general, the Nyquist radius is related to the charge transfer efficiency. And the charge transfer impedance with smaller radius is low. As shown in **Fig. 13**, the arc size of the prepared samples is observed to be

$\text{ZnWO}_4/\text{Cu}_2\text{O} < \text{Cu}_2\text{O} < \text{ZnWO}_4$. The interaction between Cu_2O and ZnWO_4 improved the electron transfer effect of $\text{ZnWO}_4/\text{Cu}_2\text{O}$ composites.

Fig. 13 Electrochemical impedance (EIS) curves of Cu_2O , ZnWO_4 and $\text{ZnWO}_4/\text{Cu}_2\text{O}$

4 Conclusions

In short, a new degradation process of 4-NP by new composite $\text{ZnWO}_4/\text{Cu}_2\text{O}$ was reported. As shown in Fig. 14. The special structure of ZnWO_4 improves the narrow band gap of Cu_2O . The electron-hole separation ability and photocatalytic activity of the composite are enhanced. In addition, during the catalytic process, ZnWO_4 quickly transferred electrons to 4-NP ions on the catalyst surface. Generate an electrically neutral 4-AP and desorb it. The active sites were transferred and the reaction could continue. The results show that the cycle utilization and stability are enhanced.

Declarations

Acknowledgements

This work was financially supported by Sichuan Province Science and Technology Support Program (2021YJ0323).

Author information

Affiliations

College of Chemical and Biological Engineering, China West Normal University, Sichuan, 637002, China (all people)

Ziwei Wang⁺¹(E-mail:2021098527@qq.com), Fengping Fu⁺(E-mail:1205160551

@qq.com), Qian He(E-mail: 2437675878@qq.com), Ting Zhu(E-mail:1627765581

@qq.com), Fang Liao*(E-mail:liaoofang407@163.com)

+1: This is senior author ; +: These authors contributed equally; *: Corresponding author

Corresponding authors

Correspondence to Fang Liao (E-mail:liaoofang407@163.com).

Statements and Declarations

Compliance with Ethical Standards

Conflict of interest

There are no conflict of interest.

Research not involving Human Participants and Animals.

known and agreed.

Bankroll

This work was financially supported by Sichuan Province Science and Technology Support Program (2021YJ0323).

References

1. Bhatt D, Gururani N, Srivastava A, et al. Sorption studies of 4-NP onto goethite: effects of contact time, pH, concentration, ionic strength and temperature[J]. *Environmental Earth Sciences*, 2021, 80(7): 273.
2. Zhang X-F, Zhu X-Y, Feng J-J, et al. Solvothermal synthesis of N-doped graphene supported PtCo nanodendrites with highly catalytic activity for 4-nitrophenol reduction[J]. *Applied Surface Science*, 2018, 428: 798-808.
3. Ghosh B K, Hazra S, Naik B, et al. Preparation of Cu nanoparticle loaded SBA-15 and their excellent catalytic activity in reduction of variety of dyes[J]. *Powder Technology*, 2015, 269: 371-378.
4. Maryam B, Nafiseh M. Biosynthesis of waste pistachio shell supported silver nanoparticles for the catalytic reduction processes[J]. *IET Nanobiotechnology*, 2018, 12(7): 939-945.
5. Suchintak D, Sourav D, Md Imran K, et al. Sonochemically synthesized Ag/CaCO₃ nanocomposites: A highly efficient reusable catalyst for reduction of 4-nitrophenol[J]. *Materials Chemistry and Physics*, 2018, 220: 409-416.
6. LUO J S, LUDWIG S, MIN-KYU S, et al. Cu₂O nanowire photocathodes for efficient and durable solar water splitting [J]. *Nano Letters*, 2016, 16(3): 1848-1857.
7. MORALES-GUIO C G, LIARDET L, MAYER M T, et al. Photoelectrochemical hydrogen production in alkaline solutions using Cu₂O coated with earth-abundant hydrogen evolution catalysts[J]. *Angewandte Chemie(International Edition)*, 2015, 54(2): 664-667.
8. Xu C, Chunxin Y, Xiaojiao G, et al. Cu₂O Nanoparticles and Multi-Branched Nanowires as Anodes for Lithium-Ion Batteries[J]. *Nano*, 2018, 13(9): 1850103.
9. Sourav G, Rituparna D, Milan Kanti N. Understanding of water-assisted template-free synthesis of Cu₂O microrods[J]. *Materials Letters*, 2017, 213: 262-265.
10. Sourav R, Matteo B, Alberto N, et al. Well-defined Cu₂O photocatalysts for solar fuels and chemicals[J]. *Journal of Materials Chemistry A*, 2021, 9: 5915-5951.
11. Hongmei W, Zhufeng L, Dingze L, et al. A surfactant-free solvothermal synthesis of Cu₂O microcrystals and their photocatalytic activity[J]. *Water Science and Technology*, 2016, 73(10): 2379-2385.
12. Gang W, Roy Van Den B, Celso De Mello D, et al. Silica-supported Cu₂O nanoparticles with tunable size for sustainable hydrogen generation[J]. *Applied Catalysis B: Environmental*, 2016, 192: 199-207.

13. Yanan G, Long Z, Arno J F V H, et al. On the surface-dependent oxidation of Cu_2O during CO oxidation: Cu^{2+} is more active than Cu^+ [J]. *Applied Catalysis A: General*, 2020, 602:117712.
14. Maryam B, Neda N, Mahmoud N. Melissa Officinalis L. leaf extract assisted green synthesis of CuO/ZnO nanocomposite for the reduction of 4-nitrophenol and Rhodamine B[J]. *Separation and Purification Technology*, 2017, 191: 295-300.
15. Akbarzadeh E, Rahman Setayesh S, Gholami M R. Investigating the role of MoS_2 /reduced graphene oxide as cocatalyst on Cu_2O activity in catalytic and photocatalytic reactions[J]. *New Journal of Chemistry*, 2017, 41(16): 7998-8005.
16. Tian L, Rui Y, Sun K, et al. Surface Decoration of ZnWO_4 Nanorods with Cu_2O Nanoparticles to Build Heterostructure with Enhanced Photocatalysis[J]. *Nanomaterials (Basel)*, 2018, 8(1): 33.
17. Coşkuner Filiz B. The role of catalyst support on activity of copper oxide nanoparticles for reduction of 4-nitrophenol[J]. *Advanced Powder Technology*, 2020, 31(9): 3845-3859.
18. Mirzaee Valadi F, Gholami M R. Synthesis of $\text{CuCo}_2\text{O}_4/\text{BiVO}_4$ composites as promise and efficient catalysts for 4-nitrophenol reduction in water: Experimental and theoretical study[J]. *Journal of Environmental Chemical Engineering*, 2021, 9(4): 105408.
19. Chang J, Bao Q, Zhang C, et al. Rapid preparation and photocatalytic properties of octahedral $\text{Cu}_2\text{O}@\text{Cu}$ powders[J]. *Advanced Powder Technology*, 2021, 32(1): 144-150.
20. Sharma A, Dutta R K, Roychowdhury A, et al. Cobalt doped CuO nanoparticles as a highly efficient heterogeneous catalyst for reduction of 4-nitrophenol to 4-aminophenol[J]. *Applied Catalysis A: General*, 2017, 543: 257-265.
21. Sasmal A K, Dutta S, Pal T. A ternary $\text{Cu}_2\text{O}-\text{Cu}-\text{CuO}$ nanocomposite: a catalyst with intriguing activity[J]. *Dalton Trans*, 2016, 45(7): 3139-50.
22. Akbarzadeh E, Rahman Setayesh S, Gholami M R. Investigating the role of MoS_2 /reduced graphene oxide as cocatalyst on Cu_2O activity in catalytic and photocatalytic reactions[J]. *New Journal of Chemistry*, 2017, 41(16): 7998-8005.
23. Akbarzadeh E, Soheili H Z, Gholami M R. Novel $\text{Cu}_2\text{O}/\text{Cu}-\text{MOF}/\text{rGO}$ is reported as highly efficient catalyst for reduction of 4-nitrophenol[J]. *Materials Chemistry and Physics*, 2019, 237: 121846.
24. Coşkuner Filiz B. The role of catalyst support on activity of copper oxide nanoparticles for reduction of 4-nitrophenol[J]. *Advanced Powder Technology*, 2020, 31(9): 3845-3859.
25. Mirzaee Valadi F, Gholami M R. Synthesis of $\text{CuCo}_2\text{O}_4/\text{BiVO}_4$ composites as promise and efficient catalysts for 4-nitrophenol reduction in water: Experimental and theoretical study[J]. *Journal of Environmental Chemical Engineering*, 2021, 9(4): 105408.
26. Das R, Sypu V S, Paumo H K, et al. Silver decorated magnetic nanocomposite ($\text{Fe}_3\text{O}_4@\text{PPy}-\text{MAA}/\text{Ag}$) as highly active catalyst towards reduction of 4-nitrophenol and toxic organic dyes[J]. *Applied Catalysis B: Environmental*, 2019, 244: 546-558.
27. Akbarzadeh E, Gholami M R. $\text{Pt}-\text{NiO}-\text{Al}_2\text{O}_3/\text{G}$ derived from graphene-supported layered double hydroxide as efficient catalyst for 4-nitrophenol reduction[J]. *Research on Chemical Intermediates*,

2017, 43(10): 5829-5839.

28. Malik M A, Alshehri A A, Patel R. Facile one-pot green synthesis of Ag–Fe bimetallic nanoparticles and their catalytic capability for 4-nitrophenol reduction[J]. Journal of Materials Research and Technology, 2021, 12: 455-470.
29. Chang J, Bao Q, Zhang C, et al. Rapid preparation and photocatalytic properties of octahedral $\text{Cu}_2\text{O}@\text{Cu}$ powders[J]. Advanced Powder Technology, 2021, 32(1): 144-150.
30. Chang J, Bao Q, Zhang C, et al. Rapid preparation and photocatalytic properties of octahedral $\text{Cu}_2\text{O}@\text{Cu}$ powders[J]. Advanced Powder Technology, 2021, 32(1): 144-150.
31. Hu Y, Yang S, Tao B, et al. Catalytic decomposition of ammonium perchlorate on hollow mesoporous CuO microspheres[J]. Vacuum, 2019, 159: 105-111.

Figures

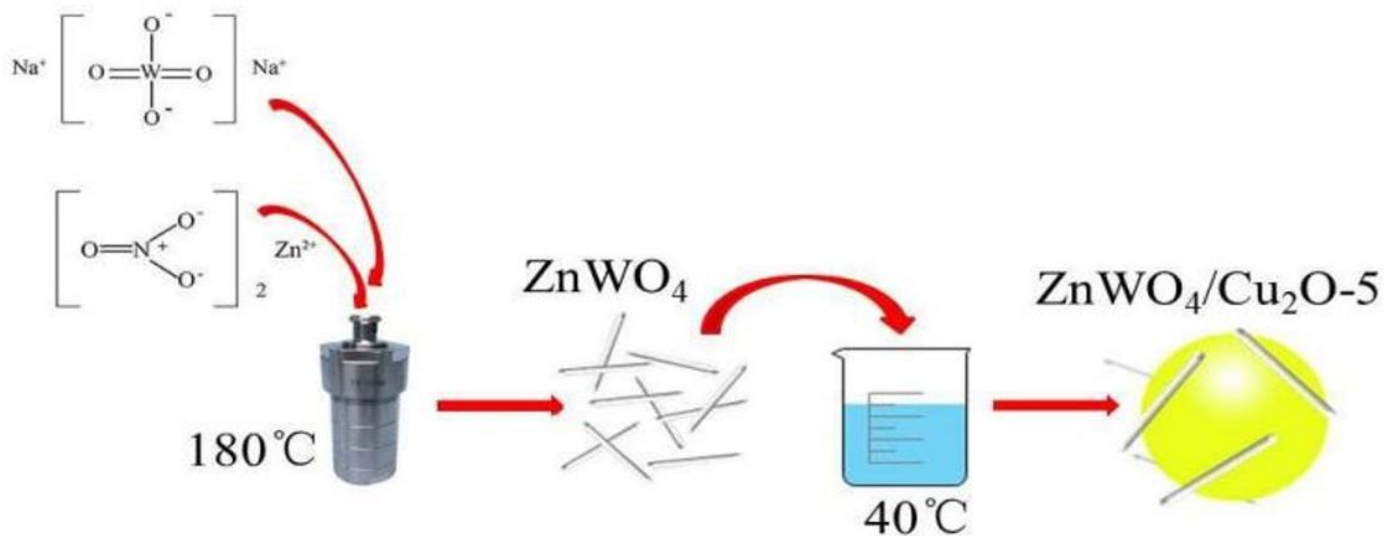


Figure 1

Preparation process of $\text{ZnWO}_4/\text{Cu}_2\text{O}$ composite

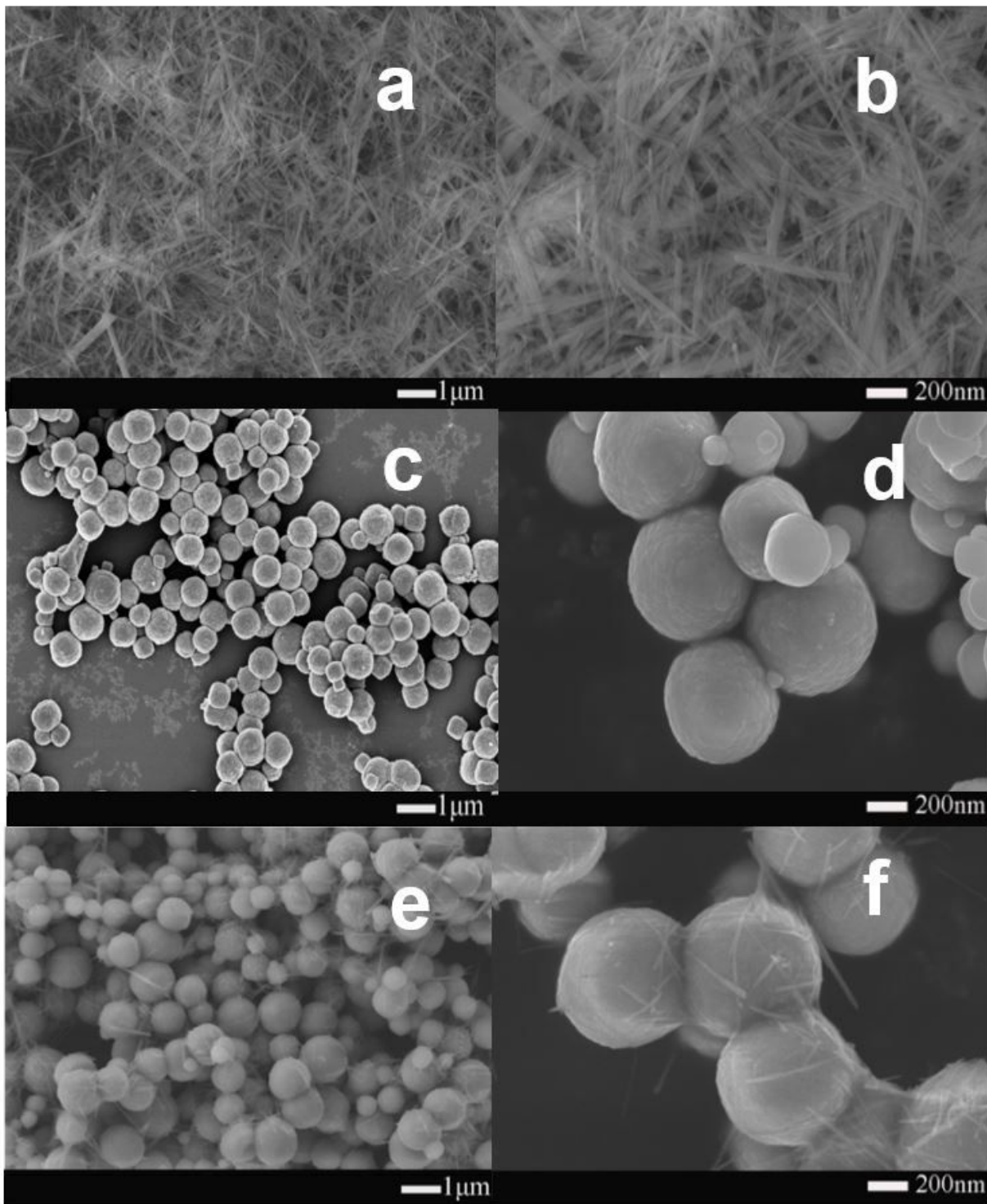


Figure 2

SEM images of (a-b) ZnWO₄; (c-d) Cu₂O; (e-f) ZnWO₄/Cu₂O

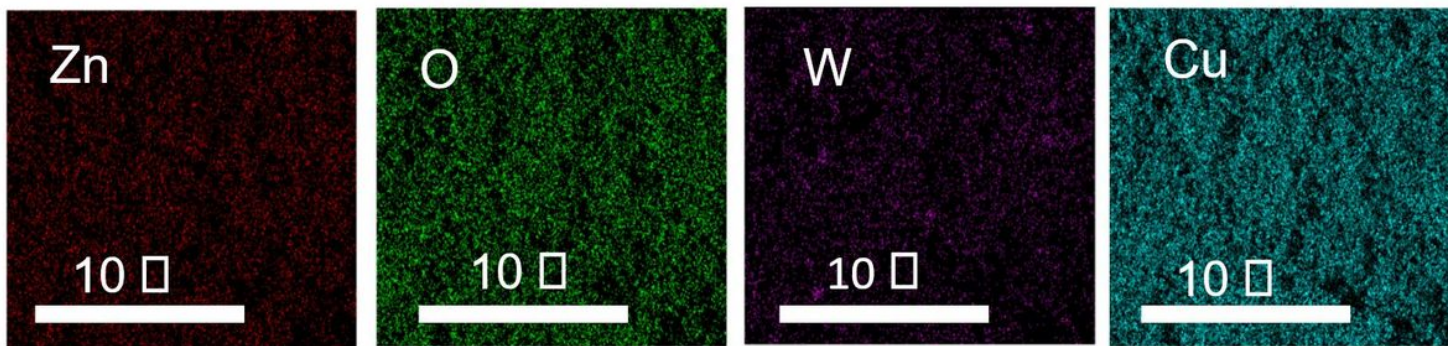


Figure 3

Mapping images of ZnWO₄/Cu₂O (Disribution of Zn, O, W and Cu)

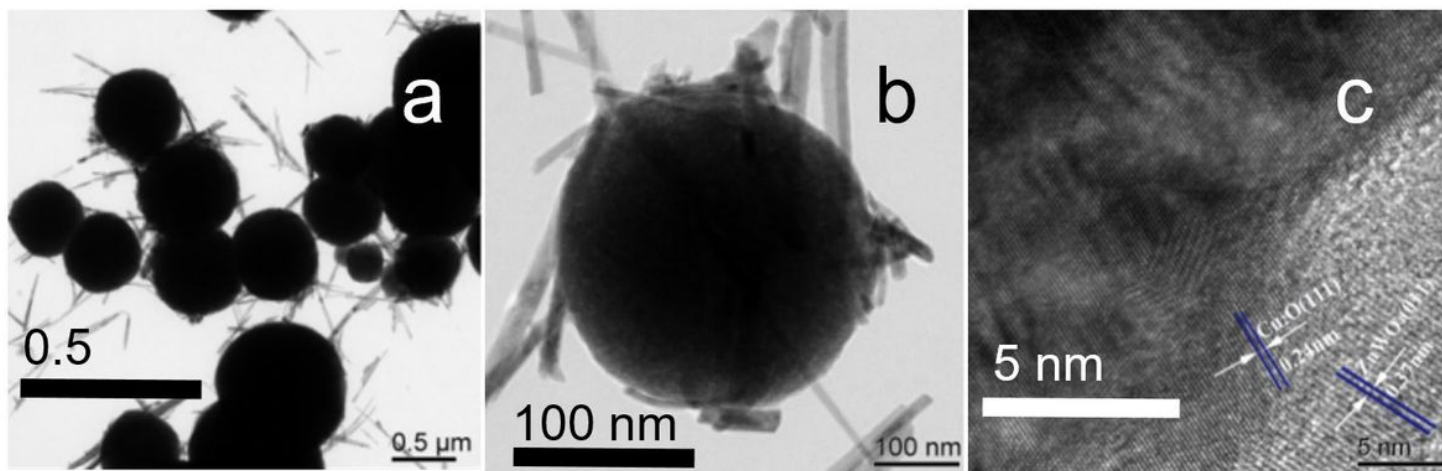


Figure 4

TEM and HRTEM images of ZnWO₄/Cu₂O

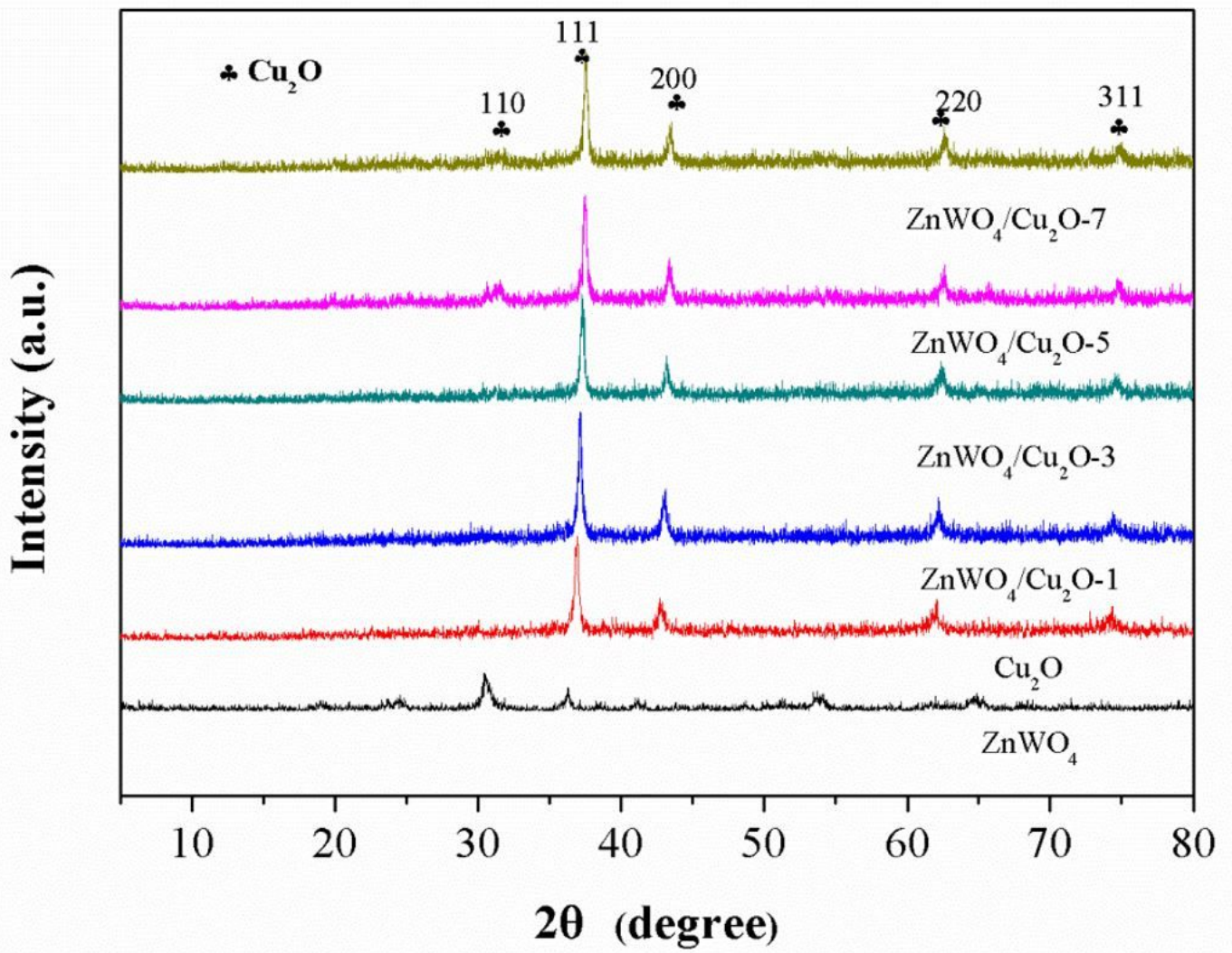


Figure 5

XRD patterns of ZnWO₄; Cu₂O; ZnWO₄/Cu₂O-X

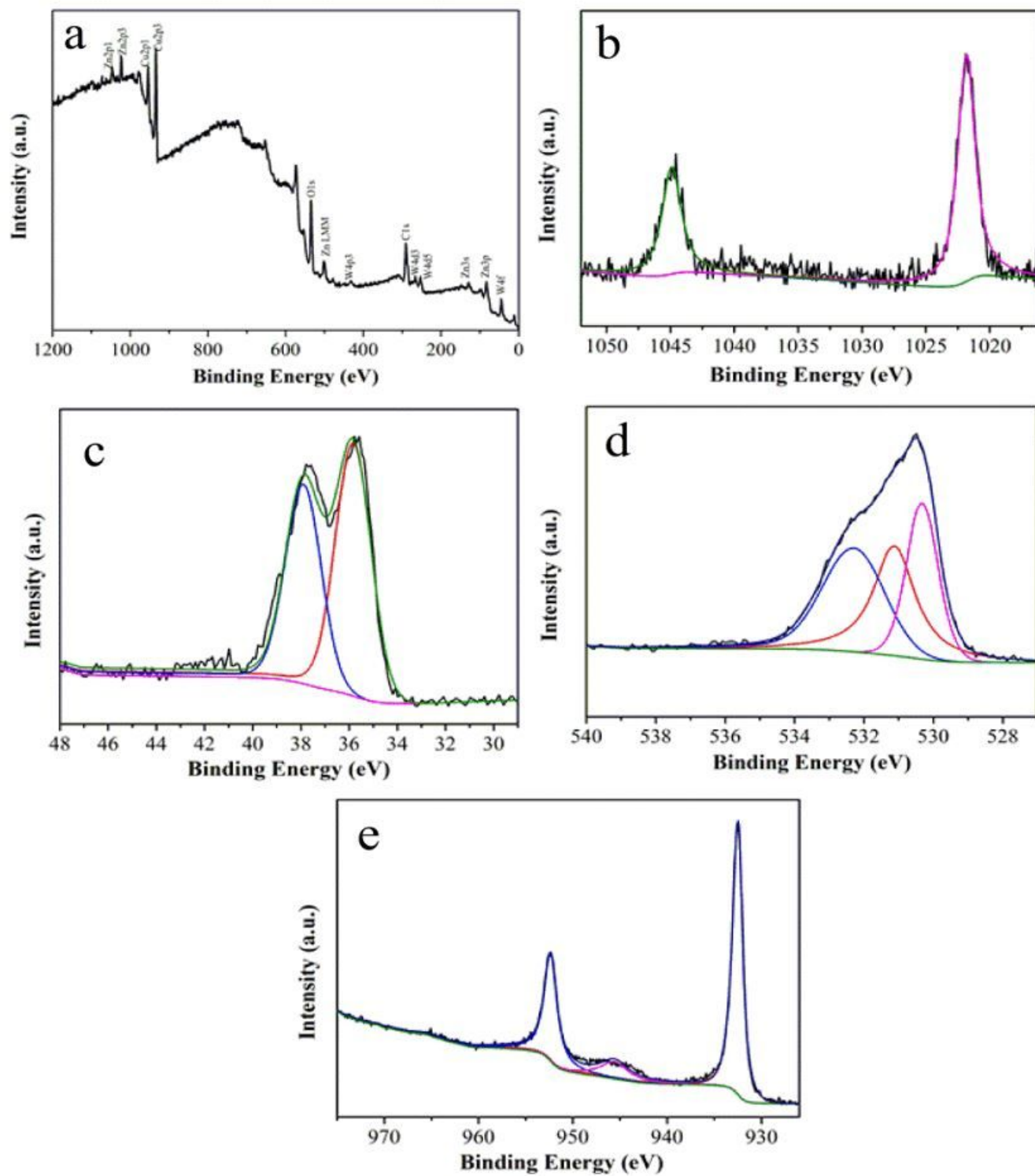


Figure 6

a XPS survey spectra; High-resolution XPS spectra of b Zn 2p; c W 4f; d O 1s and e Cu 2p

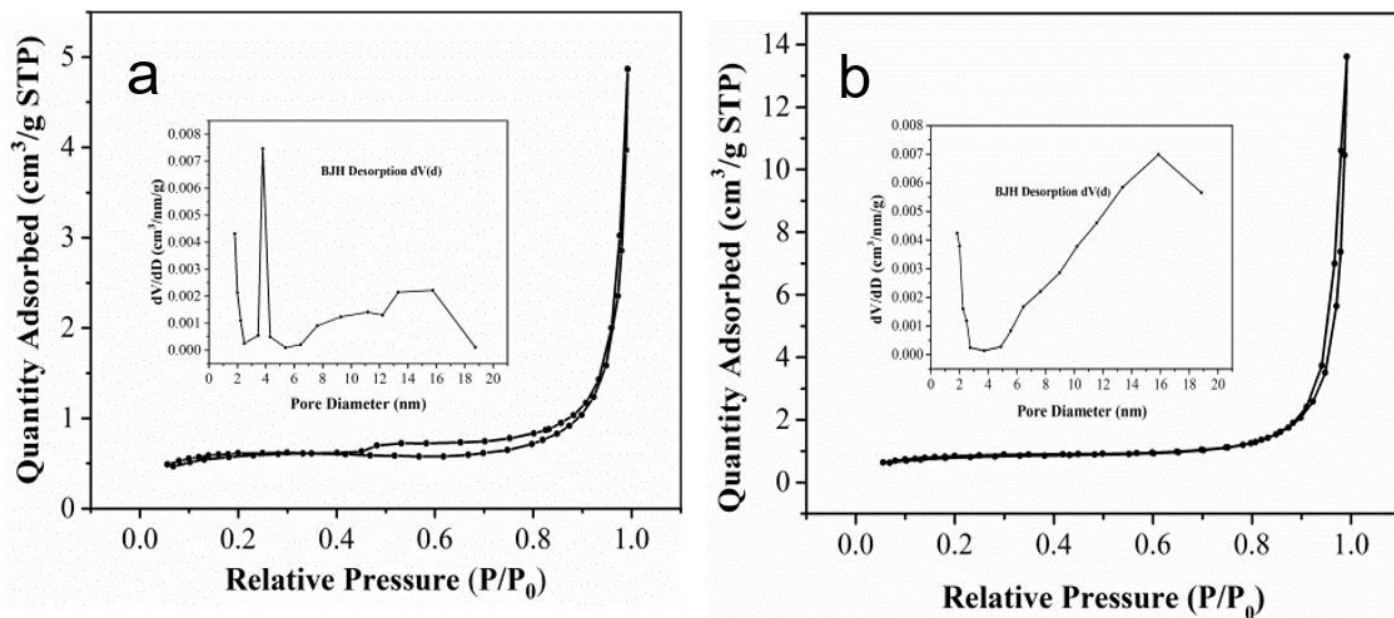


Figure 7

N₂ adsorption and desorption curves of a Cu₂O; b ZnWO₄/Cu₂O

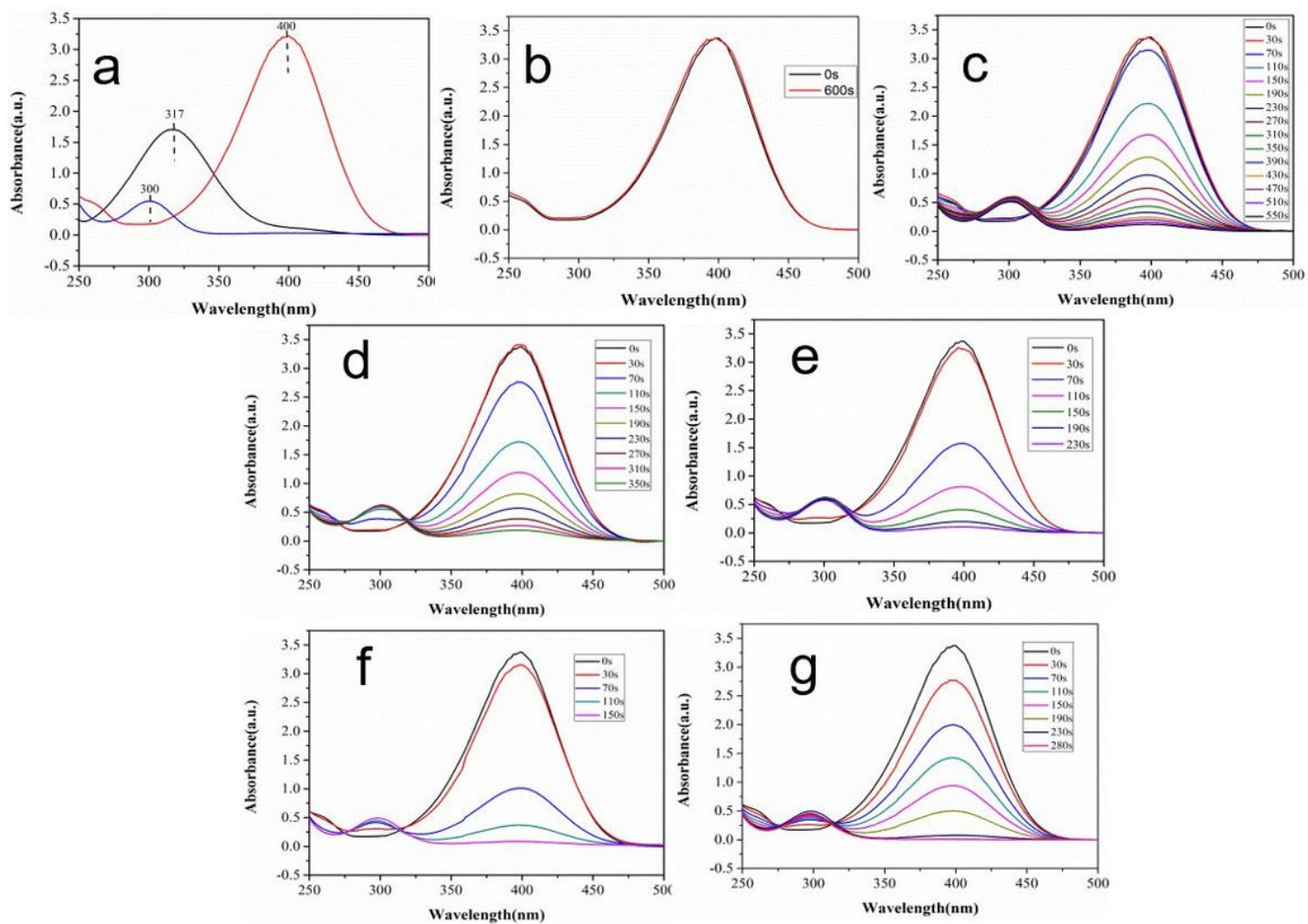


Figure 8

a UV-Vis absorption spectra of the 4-NP reaction process catalyzed by hydrogenation; UV-Vis absorption spectra of b ZnWO₄, c Cu₂O, d ZnWO₄/Cu₂O-1, e ZnWO₄/Cu₂O-3, f ZnWO₄/Cu₂O-5, g ZnWO₄/Cu₂O-7 catalytic reduction of 4-NP

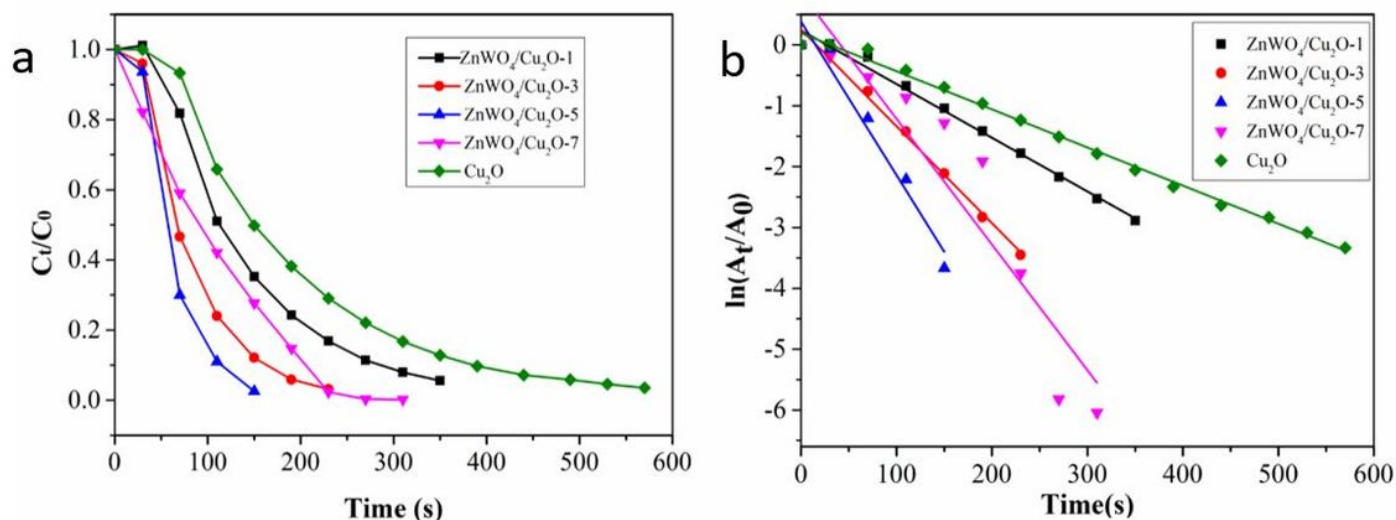


Figure 9

Different catalysts of a Ct /C0 curve graph with time; b netic fitting graph

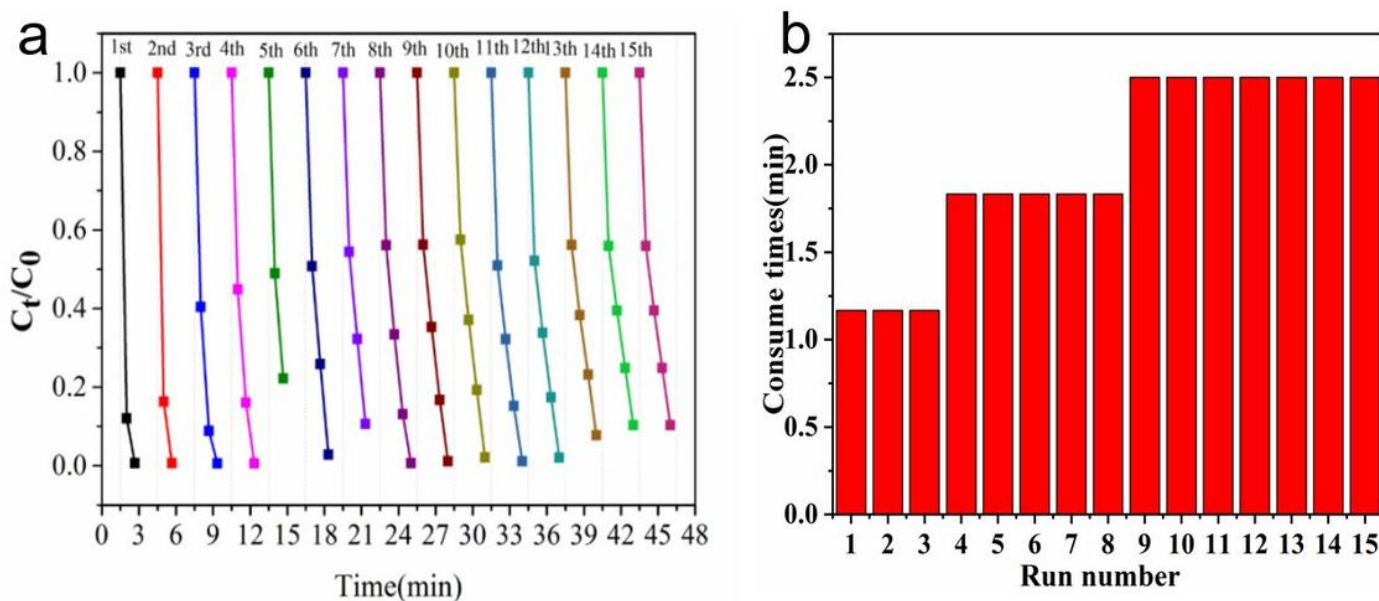


Figure 10

a The cycle stability test of ZnWO₄/Cu₂O-5 and b the time required for ZnWO₄/Cu₂O-5 to convert the same quality 4-NP

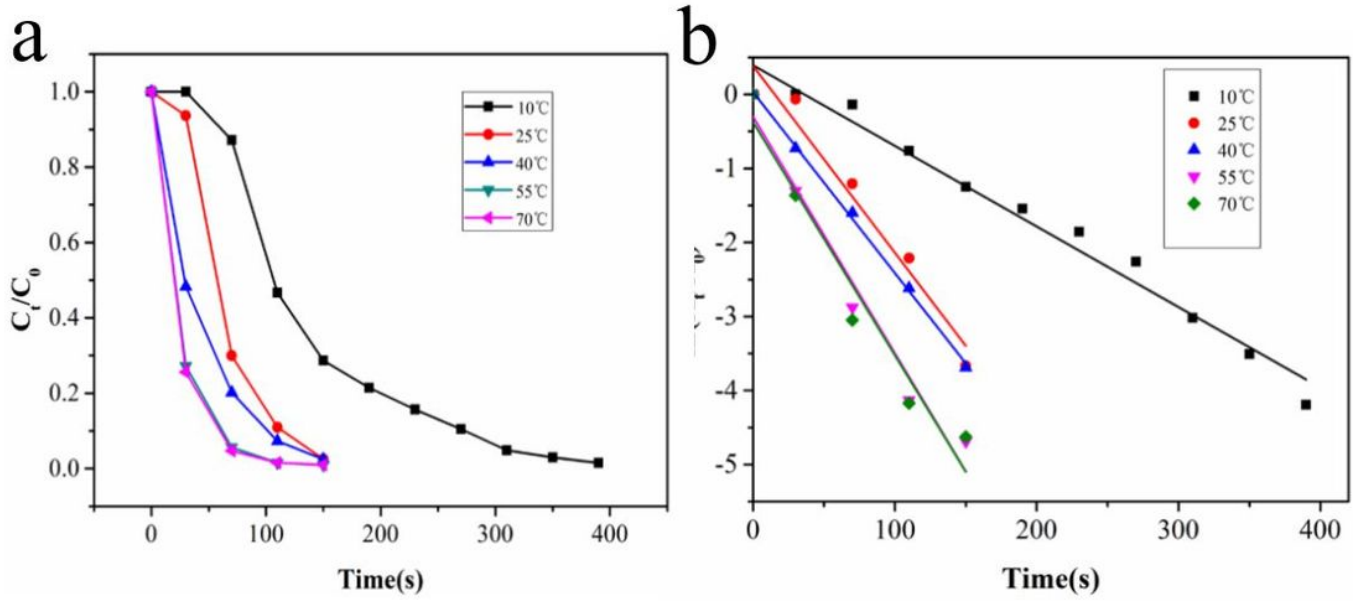


Figure 11

a The relationship between C_t/C_0 and time at different temperatures and b kinetic fitting graph

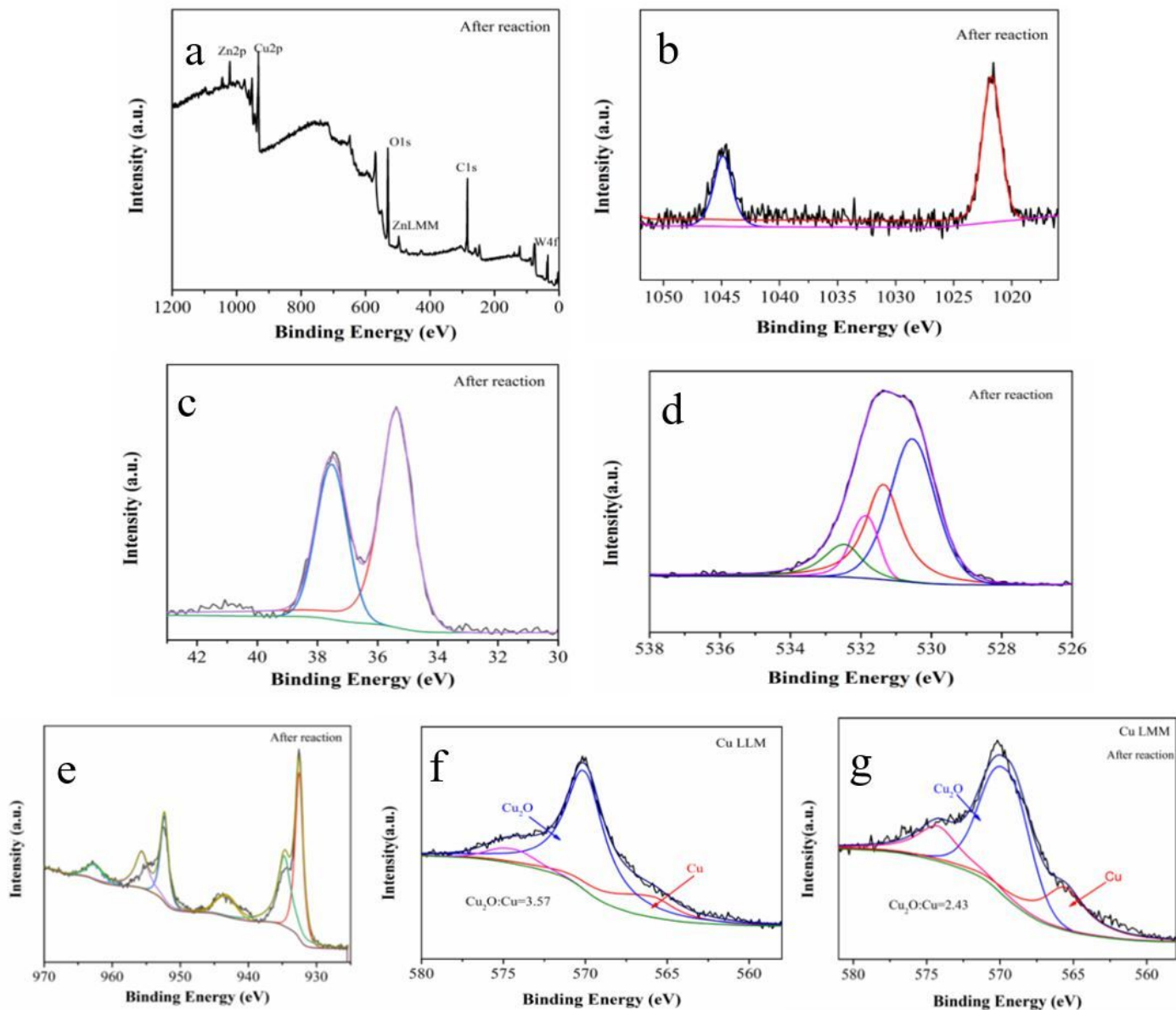


Figure 12

a The XPS survey spectrum of the recycled ZnWO₄/Cu₂O; the high-resolution XPS spectra for b Zn 2p, c W 4f, d O 1s, e Cu 2p, f Cu LMM of the refreshed and g the used Cu LMM

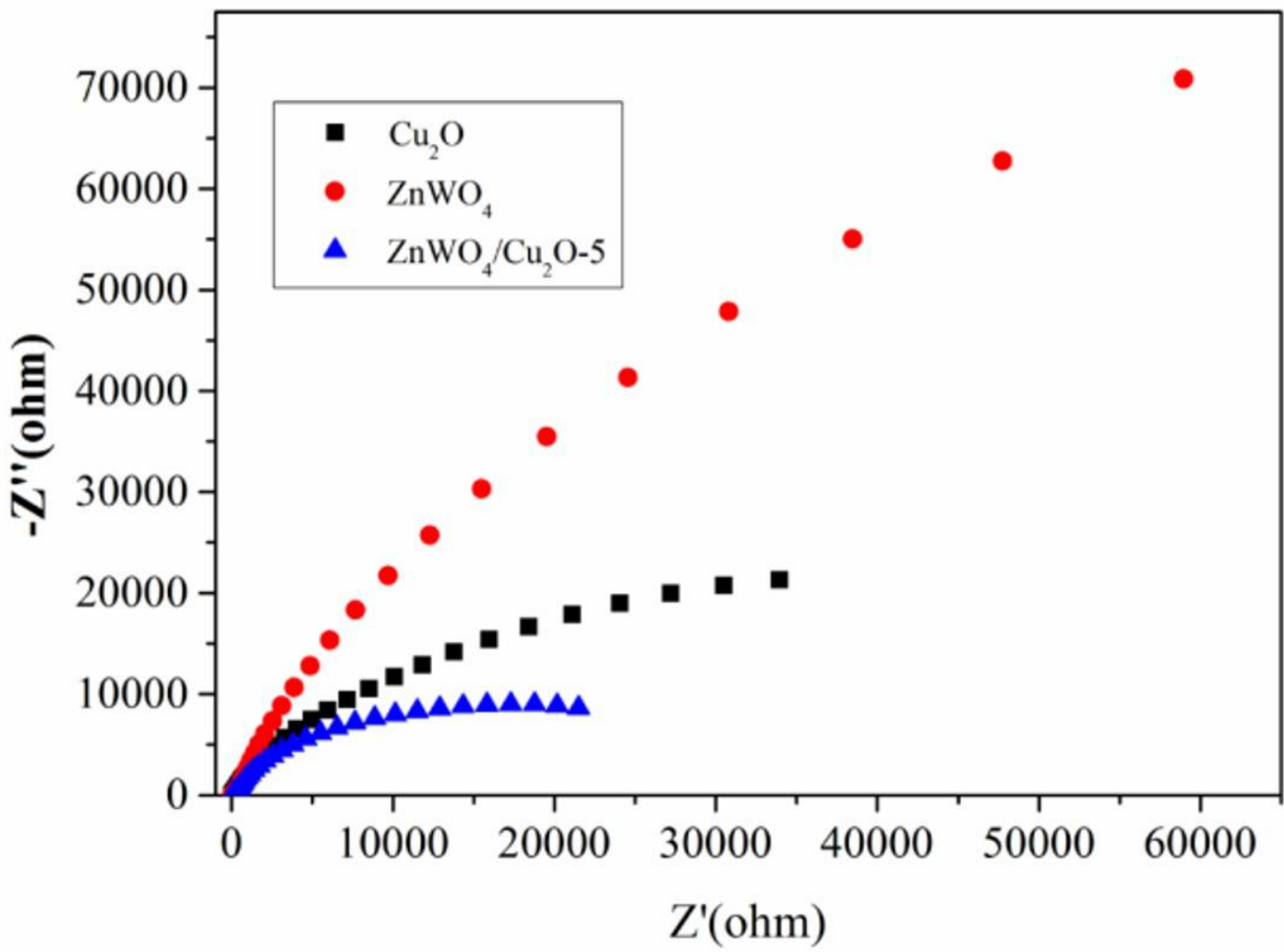


Figure 13

Electrochemical impedance (EIS) curves of Cu_2O , ZnWO_4 and $\text{ZnWO}_4/\text{Cu}_2\text{O}$

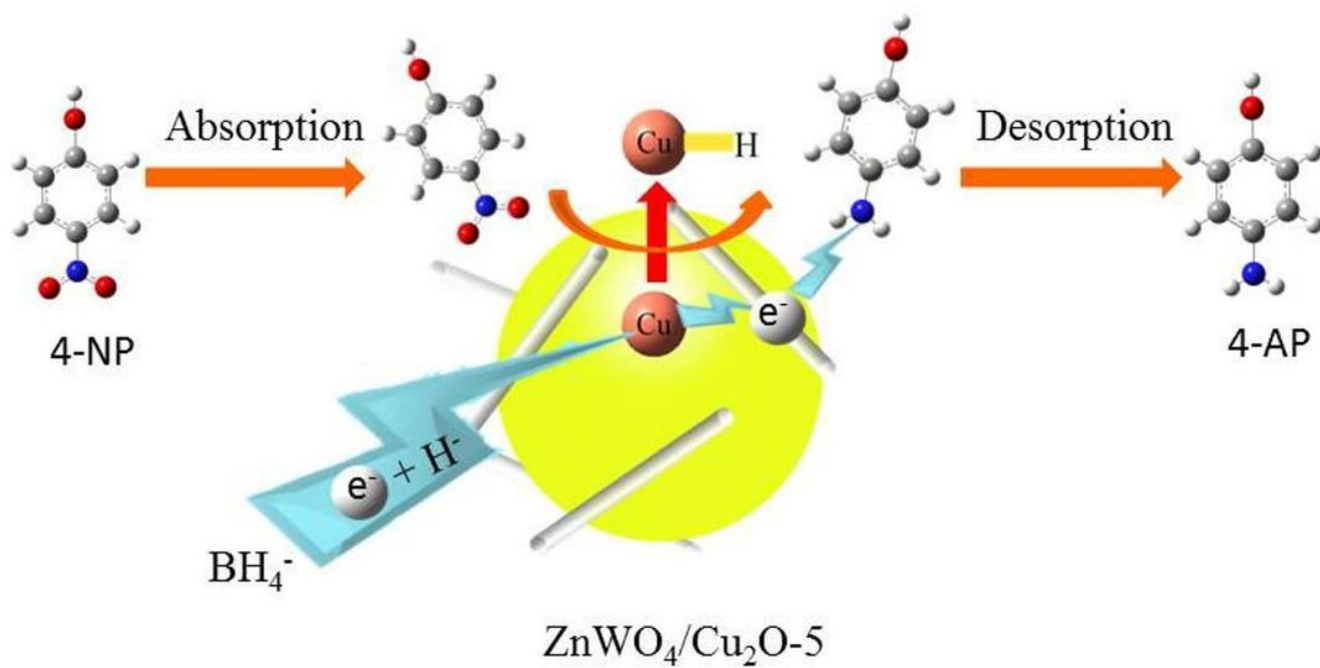


Figure 14

Diagram of the catalytic reaction mechanism of $\text{ZnWO}_4/\text{Cu}_2\text{O}$